Synthetic Gauge Phase in Rydberg Electromagnetically Induced Transparency

Ya-Dong Hu[1,2†], Yi-Chen Zhang[1,2†], Qing-Xuan Jie[1,2], Hong-Jie Fan[1,2], Xiao-Kang Zhong[1,2], Dong-Qi Ma[1,2], Ya-Nan Lv[1,2], Yan-Lei Zhang[1,2,3], Xu-Bo Zou[1,2,3], Song-Bai Kang[4], Guang-Can Guo[1,2,3], Zhu-Bo Wang[1,2*], and Chang-Ling Zou[1,2,3*]

[1]*Laboratory of Quantum Information, University of Science and Technology of China, Hefei 230026, China*
[2]*CAS Center for Excellence in Quantum Information and Quantum Physics, University of Science and Technology of China, Hefei 230026, China*
[3]*Hefei National Laboratory, University of Science and Technology of China, Hefei 230088, China*
[4]*Innovation Academy for Precision Measurement Science and Technology, Chinese Academy of Sciences, Wuhan 430071, China*

(Received 6 January 2026; accepted manuscript online 12 March 2026)

We demonstrate a synthetic gauge phase in Rydberg electromagnetically induced transparency (EIT) using room-temperature rubidium vapor. By utilizing the polarization selection rules in a ladder-type system involving ground, intermediate, and Rydberg states, multiple Zeeman sublevels form closed-loop transitions that acquire a gauge phase. We show that the relative polarization angle between the linearly polarized probe and coupling lasers directly controls the gauge phase, which modulates the EIT transmission and Rydberg state population, consequently controlling the linewidth of EIT owing to Rydberg dipole–dipole interactions between atoms. Our approach provides a simple polarization-based method for realizing synthetic gauge physics and manipulating many-body interactions in atomic ensembles without requiring laser cooling or dipole traps.

DOI: 10.1088/0256-307X/43/4/040303 CSTR: 32039.14.0256-307X.43.4.040303

1. Introduction. Since the 1990s, electromagnetically induced transparency (EIT)[1] in atomic ensembles has attracted significant attention and has become a cornerstone of quantum optics for studying light–matter interactions. EIT is a quantum interference phenomenon in which the absorption of a resonant probe beam is suppressed in the presence of a strong control field coupled to an auxiliary transition. The underlying mechanism involves destructive interference between different excitation pathways, which creates a narrow transparency window accompanied by a sharp modulation of the dispersion. When the light–atom interaction is extended from individual atoms to atomic ensembles, EIT gives rise to collective phenomena, where the probe photon couples to collective atomic excitations, for example, spin waves. Nonpropagating and long-coherence spin waves enable coherent information storage[2–4] and drastically reduce the group velocity of light.[5] The universality of EIT as a coherent interference phenomenon has been extended to diverse physical platforms, including optomechanical systems,[6] superconducting quantum circuits,[7] solid-state defects,[8] and plasmonic nanostructures.[9]

The textbook treatment of EIT typically employs a simplified three-level model. However, real atoms possess a rich internal structure with multiple hyperfine and Zeeman sublevels, offering opportunities to extend EIT physics in two complementary directions. First, the incorporation of highly excited Rydberg states into the ladder scheme introduces strong long-range dipole–dipole interactions. This Rydberg EIT platform has revealed fascinating many-body phenomena, including dipole blockade,[10] single-photon nonlinearity,[11] and optical bistability,[12] demonstrating the potential of atoms as a powerful medium for quantum simulation[13–20] and electric field measurements.[21–23] Second, the multilevel structure enables multiple coherent pathways to connect the same initial and final states. When the excitation pathways form closed loops, another interference effect emerges from the phase accumulated around the loop, which constitutes a synthetic gauge phase[24–29] analogous to the Aharonov–Bohm phase acquired by charged particles encircling the magnetic flux. The synthetic gauge phase has also been realized in atomic systems through other methods, including laser-assisted tunneling in ultracold atomic optical lattices,[30] employing the internal states of fermions and bosons as a synthetic dimension to observe chiral edge states,[31,32] synthetic dimensions and spin–orbit coupling based on clock transitions,[33] and momentum-space superradiant lattices in room-temperature atoms.[34] Unlike conventional synthetic gauge fields, which require ultracold atoms in optical lattices and tweezer arrays,[26,35–37] such internal-state loops offer an alternative route for gauging physics in simple atomic ensembles.

In this letter, we demonstrate a synthetic gauge phase

†These authors contributed equally to this work.
*Corresponding authors. Email: zbwang@ustc.edu.cn; clzou321@ustc.edu.cn
© 2026 Chinese Physical Society and IOP Publishing Ltd. All rights, including for text and data mining, AI training, and similar technologies, are reserved.

in Rydberg EIT by utilizing both extensions simultaneously, employing Rydberg interactions and closed-loop transitions among Zeeman sublevels. Using rubidium vapor at room temperature, we showed that the relative polarization angle between the linearly polarized probe and the coupling lasers directly controls the gauge phase. As this angle varies, sinusoidal oscillations are observed in both the EIT transmission intensity and linewidth, providing direct evidence of the gauge phase. This mechanism provides an additional control parameter that modulates the Rydberg state population through EIT interference and thus controls the strength of the dipole–dipole interactions among Rydberg atoms. The demonstration of the gauge phase through simple polarization control provides a knob for exploring new phenomena and applications in atomic ensembles.

2. Model. Figure 1(a) illustrates a diamond-type energy-level diagram for Rydberg EIT, where the probe and coupling lasers couple the ground state $|g\rangle$ to the Rydberg state $|r\rangle$ through two intermediate states $|e_1\rangle$ and $|e_2\rangle$ simultaneously. The two ladder-type EIT transitions lead to interference, that is, the absorption of the probe laser, and the generated Rydberg state population shows destructive or constructive interference, depending on the relative phase between the two paths. Equivalently, the diamond-type Rydberg EIT produces a loop of transitions, and a synthetic magnetic flux emerges in the loop that controls the population transfer among energy levels. The system dynamics can be described using the Hamiltonian and master equations[38,39]

$$\begin{aligned}\mathcal{H} = {} & \delta_{\rm eff}|g\rangle\langle g| + \Omega_{\rm p}(\mathrm{e}^{\mathrm{i}\psi_1}|e_1\rangle\langle g| + \mathrm{e}^{\mathrm{i}\psi_2}|e_2\rangle\langle g|) \\ & + \Omega_{\rm c}(\mathrm{e}^{\mathrm{i}\phi_1}|r\rangle\langle e_1| + \mathrm{e}^{\mathrm{i}\phi_2}|r\rangle\langle e_2|) + \text{H.c.}, \qquad (1)\end{aligned}$$

$$\dot{\rho} = \frac{1}{\mathrm{i}\hbar}[\mathcal{H}, \rho] + \sum_k \left(L_k \rho L_k^\dagger - \frac{1}{2}\{L_k^\dagger L_k, \rho\}\right). \qquad (2)$$

Here, $\Omega_{\rm p}$ and $\Omega_{\rm c}$ are the Rabi frequencies of the probe and coupling lasers, respectively, which are set to $2\pi \times 10\,\text{kHz}$ and $2\pi \times 100\,\text{kHz}$, respectively, in the following simulations. The associate decoherence processes are described by the Lindblad terms $\{L_k\} = \{\sqrt{\kappa_{\rm e}}|g\rangle\langle e_1|, \sqrt{\kappa_{\rm e}}|g\rangle\langle e_2|, \sqrt{\frac{\kappa_{\rm r}}{2}}|e_1\rangle\langle r|, \sqrt{\frac{\kappa_{\rm r}}{2}}|e_2\rangle\langle r|\}$. Here, $\kappa_{\rm e}$ and $\kappa_{\rm r}$ denote the decay rates of the intermediate and Rydberg states, respectively. In our simulations, we set $\kappa_{\rm e} = 2\pi \times 1.3\,\text{MHz}$ and $\kappa_{\rm r} = 2\pi \times 10\,\text{kHz}$. A key feature of this energy structure is that the couplings form a closed loop. In general, when the couplings among the internal states do not form a loop, the driving phases can be effectively eliminated by redefining the internal states without affecting the properties of the system. However, when a loop exists, the accumulated phases cannot be eliminated and directly affect the properties of the system.[25,28] Owing to the gauge invariance, we can study it using a gauge-phase approach. The synthetic gauge phase θ of this system is defined as the accumulated phase of the drives around the loop $\theta = \phi_2 - \phi_1 + \psi_2 - \psi_1$. We set ϕ_2, ψ_1, and ψ_2 to zero and control the gauge phase by ϕ_1 in the simulation. To study the influence of the Rydberg interaction on the synthetic gauge phase, we introduce mean field theory[38] to simplify the many-body dynamics in an atomic ensemble. The model introduces a mean field shift $\delta_{\rm eff} = \delta + \eta\rho_{\rm rr}$, which contains a term proportional to the Rydberg population $\rho_{\rm rr}$ with coefficient η.

We numerically calculated the transmission of the probe based on the steady-state solution of the master equation[38,39] [Fig. 1(b)]. The effective atomic density was derived from the saturation vapor pressure of ^{87}Rb at 370 K.[40] We then estimated the mean-field coefficient η using the effective atomic density and Rydberg interaction strength, $V = C_6/r^6$,[41] where r is the interatomic distance. When $\theta = 0$ and $\eta = 0$, the system exhibits a standard structure of ladder-type EIT, exhibiting a narrow transparent window within a broad absorption valley, as illustrated in Fig. 1(c). The transparent window disappears when $\theta = \pi$. As the gauge phase is fine-tuned, the results in Fig. 1(d) show the gradual change in the peak transmission values. In Fig. 1(e), we extract the transmission peak $T_{\rm peak}$ of the EIT window, which shows sinusoidal oscillations with θ. Furthermore, Fig. 1(d) compares the results of the system with and without Rydberg interaction. We observed that, when we have a finite Rydberg interaction strength (here, we set $\eta = 2\pi \times 5\,\text{MHz}$), the Hamiltonian becomes nonlinear, leading to asymmetric transmission lineshapes and a shift in the resonance frequency. We characterized the nonlinear effect by calculating the maximum slope of the transmission $|\partial T/\partial\delta|_{\rm max}$. Figure 1(f) shows that, when the interaction strength is finite, the maximum slope oscillates with a larger amplitude as a function of the gauge phase θ, indicating an interplay between the gauge phase and the atom–atom interactions.

3. Experimental Setup. Figure 2(a) shows the experimental setup used to study Rydberg EIT in ^{87}Rb atomic vapor (370 K). The setup comprises two laser sources: a weak 420 nm probe laser coupling the ground state $|g\rangle = |5\text{S}_{1/2}, F = 2\rangle$ to the intermediate state $|e\rangle = |6\text{P}_{3/2}, F = 3\rangle$, and a strong 1013 nm coupling laser driving the transition between $|e\rangle$ and the Rydberg state $|r\rangle = |70\text{S}_{1/2}\rangle$, with the corresponding energy-level diagram shown in Fig. 2(b). The probe laser beam had a diameter of 1.5 mm and a power of 1 mW. The coupling-beam diameter was 2.7 mm. The Rabi frequency of the coupling drive $\Omega_{\rm c}$, which is proportional to $\sqrt{P_{\rm c}}$, was tuned by varying the coupling power $P_{\rm c}$ over the range from 16 mW to 190 mW.

There are several Zeeman sublevels, and the probe and coupling lasers can simultaneously couple to these energy levels with different coupling strengths. When both lasers are linearly polarized, they can be decomposed into superpositions of left- (σ^-) and right-circularly (σ^+) polarized components. According to the transition selection rules, there are closed loops exist in which a combination of σ^+-σ^- or σ^--σ^+ cascaded probe-coupling transitions can interfere, as highlighted by the red and blue arrows in Fig. 2(b). Thus, two linearly polarized lasers can simultaneously form numerous closed loops. As all dipole moment coupling $|g\rangle \leftrightarrow |e\rangle$ and $|e\rangle \leftrightarrow |r\rangle$ transitions have the same sign, each closed loop acquires the same synthetic gauge phase θ, which is determined by the relative polarization

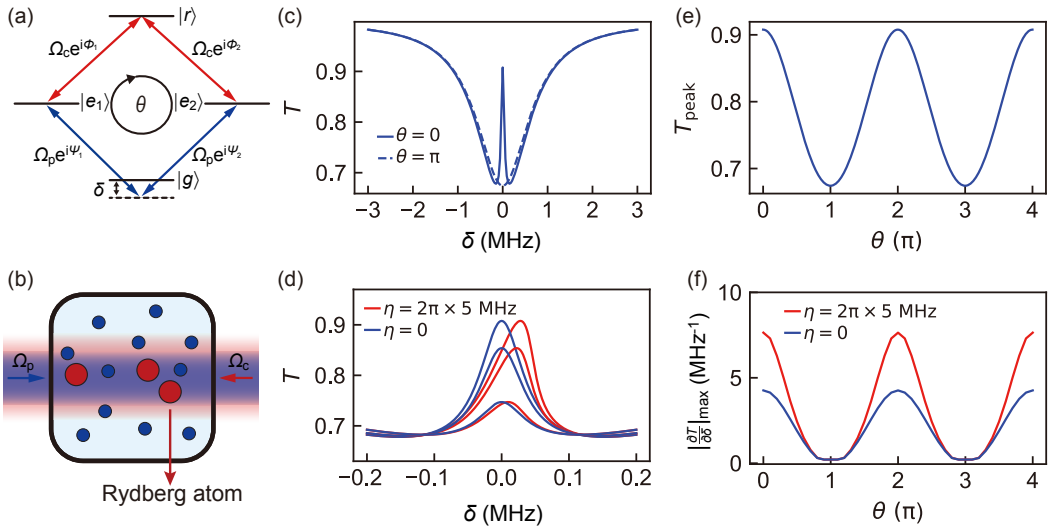

Fig. 1. (a) Diamond-type energy-level configuration for Rydberg EIT, with synthetic gauge phase θ accumulated in a closed-loop transition. (b) Schematic of counterpropagating probe and control lasers interacting with Rydberg atom ensemble in a vapor cell. (c) Transmission (T) spectra for $\theta = 0$ (solid line) and $\theta = \pi$ (dashed line). (d) EIT spectra with (red line) and without (blue line) Rydberg interaction for $\theta = 0,\ 0.3\pi,\ 0.6\pi$ (top to bottom). (e) EIT transmission peak as a function of θ. (f) Maximum transmission slope versus θ with (red line) and without (blue line) Rydberg interaction.

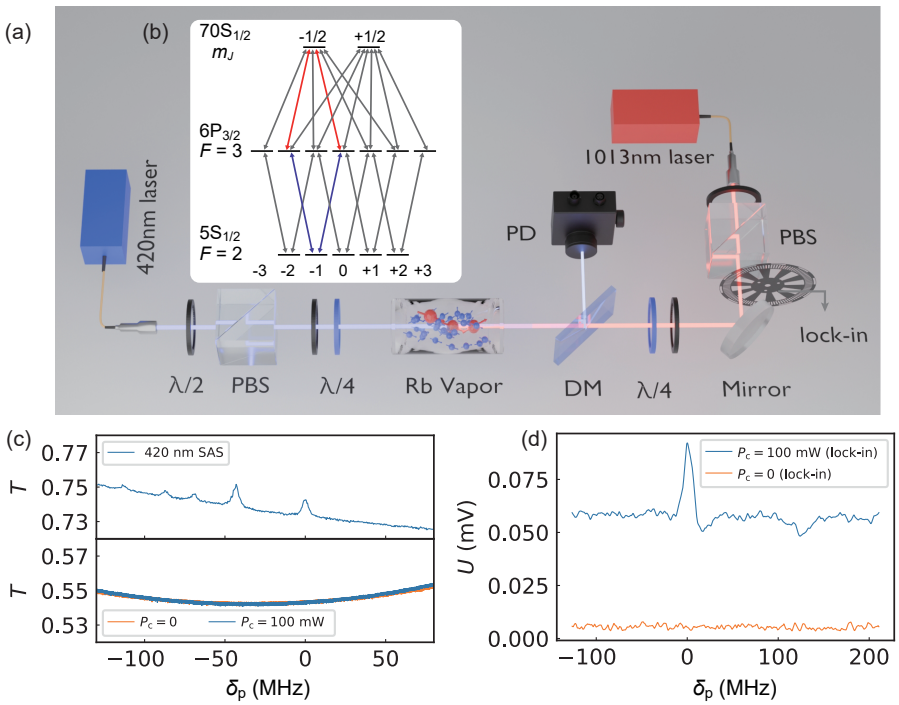

Fig. 2. (a) Schematic of the experimental setup. PBS: polarization beam splitter; HWP: half-wave plate; QWP: quarter-wave plate; DM: dichroic mirror; PD: photodiode. (b) Relevant energy levels of rubidium atoms. (c) Saturated absorption spectrum (SAS) (top) and probe absorption profile (bottom) obtained by scanning the probe laser detuning (δ_p), with and without coupling laser ($P_c = 100\,\text{mW}$). (d) EIT spectrum versus probe laser detuning, with the coupling laser frequency locked to the $|6P_{3/2}, F = 3\rangle \rightarrow |70S_{1/2}\rangle$ transition. EIT signals are detected using lock-in amplification with modulation acting on the coupling laser while the frequency of the coupling laser and the intensity of the probe laser are fixed. The probe and coupling laser powers are 1 mW and 100 mW (0 mW), with horizontal and left circular polarizations, respectively. The EIT signal is acquired as the voltage U.

angle between the probe and coupling fields. Although differences in the dipole moments affect the oscillation contrast between the EIT peak value and the gauge phase, the effective four-level model presented above is sufficient to demonstrate the primary properties. To implement a precise polarization control, we employed polarization beam splitters (PBSs) to purify the initial polarization states of both beams. Half-wave plates (HWPs) allowed the continuous rotation of the linear polarization orientation, whereas a quarter-wave plate (QWP) enabled switching to circular polarization for the control experiments. The two beams counterpropagated through a heated vapor cell and

were subsequently separated by a dichroic mirror (DM). The transmitted probe signal (U) was detected using a silicon avalanche photodiode (PD).

To investigate the Rydberg EIT, we first calibrated the probe laser detuning using the saturated absorption spectrum (SAS),[42] as shown in the top panel of Fig. 2(c). However, the EIT signal could not be directly detected for a weak transition [bottom panel of Fig. 2(c)]. Thus, we employed the lock-in amplification technique,[43] where 130 kHz intensity modulation was introduced into the coupling laser through an acousto-optic modulator, and the EIT signal-to-noise ratio could be enhanced by extracting the modulation of the transmission. Figure 2(d) shows the experimentally observed Rydberg EIT spectrum with $P_c = 100$ mW, where the probe light is horizontally (H) polarized and the coupling light is circularly polarized, preventing the formation of closed loops of transitions. Here, the EIT spectral profile shows distinct asymmetry, attributed to Rydberg interactions between atoms,[21] as predicted in Fig. 1(d).

4. Gauge Phase. Using this experimental setup, we systematically investigated the polarization dependence of Rydberg EIT to reveal the synthetic gauge phases. Figure 3(a) shows the probe and control laser polarizations used to verify the gauge phase. With the probe laser fixed at H polarization, we systematically rotate the angle of the linearly polarized coupling laser using a motorized half-wave plate and record the EIT spectrum at each angle by scanning the coupling laser detuning (δ_c), in contrast to the results in Fig. 3(b), where the coupling was circularly polarized. As shown in Fig. 3(b), curves (i)–(iii) show the results for the angle between the control and probe polarizations of 0 (parallel, H-polarized), $\pi/4$, and $\pi/2$ (perpendicular, V-polarized), with a smaller angle showing a weaker EIT peak value.

This modulation confirmed that the relative polarization angle governs the EIT transmission. Based on the transitions shown in Fig. 1(a), we determined that the gauge phase θ is equal to twice the angle between the two linearly polarized lasers, irrespective of the polarization direction of either the probe or coupling laser. Thus, we obtain $\theta = 0$ for parallel polarizations, as both transition paths from the ground state to the Rydberg state have the same phase, whereas $\theta = \pi$ for perpendicular polarizations, and the two transition paths exhibit destructive interference.

By carefully scanning the angle, we obtained the dependence of the EIT peak voltage on the gauge phase θ. As shown in Fig. 3(c), the experimental data show sinusoidal oscillations and agree with theoretical expectations. To unambiguously verify that the observed oscillations originate from the closed-loop transition geometry, we performed an experiment by switching the input coupling laser from an initial linear polarization to a right-handed circular polarization while rotating the direction of the linearly polarized probe laser. The EIT peak value has negligible dependence on the gauge phase, confirming that the synthetic gauge phase is generated by the closed-loop transitions induced by two linearly polarized lasers.

The features of the Rydberg interactions among the atoms are shown in Fig. 4. First, for the configuration

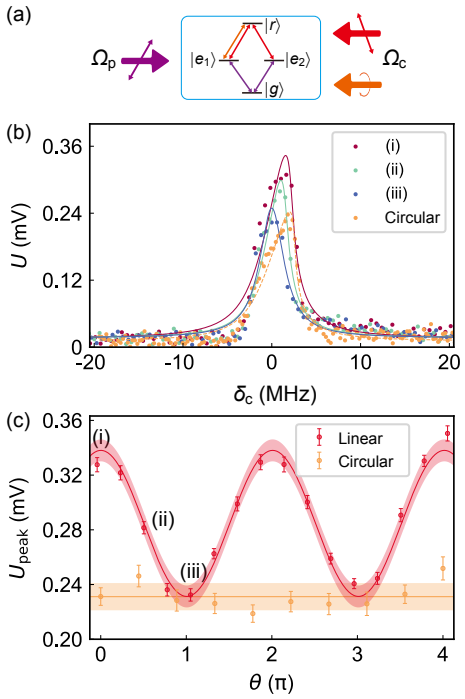

Fig. 3. (a) Level diagram depicting excitation by a linear probe (purple) and a linear (red) or left circular (orange) coupling field. (b) EIT spectra for (i) parallel (H-H), (ii) intermediate, and (iii) perpendicular (H-V) alignment between the linear polarization directions of coupling and probe lasers, and the circularly polarized coupling laser EIT spectra as shown, where δ_c is the coupling laser detuning. (c) EIT peak amplitude (U_{peak}) versus the gauge phase θ, which is derived as two times the relative polarization angle between coupling and probe lasers.

shown in Fig. 3, the EIT linewidth also exhibits a sinusoidal oscillation with a gauge phase for two linearly polarized inputs, whereas the oscillation is hardly visible in the experimental data for a circularly polarized control laser. The synchronized oscillation of the linewidth and EIT peak confirms that a stronger Rydberg population in the atomic ensemble leads to the broadening of the transition. In Fig. 4(b), we examine the interplay between the peak value and the linewidth of EIT lineshape by increasing P_c from 16 mW to 190 mW, where both the probe and coupling lasers are H-polarized. As P_c increases, the peak value becomes more significant and the linewidth broadens.

The effect of the synthetic gauge phase on the Rydberg interactions is shown in Fig. 4(c) by comparing the EIT transmissions for $\theta = 0$ (parallel polarization) and $\theta = \pi$ (perpendicular polarization) across a range of coupling powers. Throughout the power range, the $\theta = 0$ case consistently yielded a higher transmission, and the effect was more pronounced in the high-power regime, where the Rydberg interaction was stronger. Figure 4(d) shows a more quantitative presentation of the Rydberg-interaction-induced nonlinear asymmetric spectral response in EIT, that is, the maximum slope $|\partial T/\partial\delta|_{max}$. The results reveal an apparent sinusoidal modulation with θ, validating our theoretical prediction shown in Fig. 1(f), which demonstrates that the gauge phase actively regulates the effective Rydberg nonlinearity.

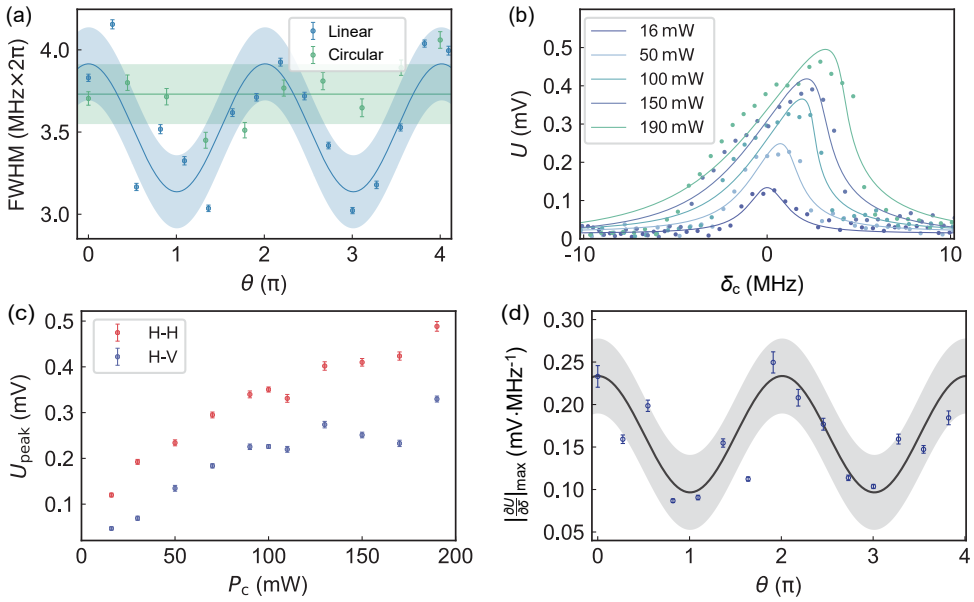

Fig. 4. (a) EIT linewidth versus θ for linear (blue) and circular (red) polarized coupling lasers. (b) Rydberg EIT spectra (H-H polarization configuration) for different coupling laser powers P_c. (c) Rydberg EIT peak transmission versus P_c for parallel (H-H, blue) and perpendicular (H-V, red) polarization configurations. (d) Maximum spectral slope versus θ.

5. Conclusion. We demonstrated a synthetic gauge phase in the Rydberg transitions of a rubidium atomic ensemble. The gauge phase modulates the Rydberg EIT spectral profile and effectively tunes the Rydberg nonlinearity by varying the laser linear polarization direction without requiring changes in the laser intensity or frequency. Experiments with a circularly polarized coupling laser validated that closed-loop transitions are essential for observing such a dependence on the gauge phase. Therefore, our study reveals polarization as an experimental control knob for manipulating both light–matter interactions and Rydberg atom–atom interactions. Although we did not observe the gauge phase modulating the physical phenomena associated with strong Rydberg interactions, such as optical bistability and nonlinear oscillations, in our current experiment, we anticipate that the gauge phase would remain effective under such conditions, which warrants further investigation in future studies. The synthetic gauge phase establishes a powerful control mechanism for exploring quantum simulations and topological phenomena.[13–20,44]

Acknowledgments. This work was supported by the National Key R&D Program (Grant No. 2021YFA1402004), the Natural Science Foundation of Anhui Province (Grant No. 2408085QA017), and the National Natural Science Foundation of China (Grant Nos. 92465201 and 12504569). Y.-N.L. was supported by the China Postdoctoral Science Foundation (Grant No. 2024M753081). This work was also supported by the Fundamental Research Funds for Central Universities and USTC Research Funds of the Double First-Class Initiative. The numerical calculations in this study were performed using a supercomputing system at the Supercomputing Center of USTC. This work was partially conducted at the USTC Center for Micro and Nanoscale Research and Fabrication.

References

[1] Boller K J, Imamoğlu A, and Harris S E 1991 *Phys. Rev. Lett.* **66** 2593
[2] Fleischhauer M and Lukin M D 2000 *Phys. Rev. Lett.* **84** 5094
[3] Phillips D F, Fleischhauer A, Mair A, Walsworth R L, and Lukin M D 2001 *Phys. Rev. Lett.* **86** 783
[4] Wang Y, Li J, Zhang S, Su K, Zhou Y, Liao K, Du S, Yan H, and Zhu S L 2019 *Nat. Photonics* **13** 346
[5] Kash M M, Sautenkov V A, Zibrov A S, Hollberg L, Welch G R, Lukin M D, Rostovtsev Y, Fry E S, and Scully M O 1999 *Phys. Rev. Lett.* **82** 5229
[6] Safavi-Naeini A H, Alegre T P M, Chan J, Eichenfield M, Winger M, Lin Q, Hill J T, Chang D E, and Painter O 2011 *Nature* **472** 69
[7] Chu K I, Lu X C, Chiang K H, Lin Y H, Chen C D, Yu I A, Liao W T, and Chen Y F 2025 *Phys. Rev. Res.* **7** L012015
[8] Turukhin A V, Sudarshanam V S, Shahriar M S, Musser J A, Ham B S, and Hemmer P R 2001 *Phys. Rev. Lett.* **88** 023602
[9] Liu N, Langguth L, Weiss T, Kästel J, Fleischhauer M, Pfau T, and Giessen H 2009 *Nat. Mater.* **8** 758
[10] Lukin M D, Fleischhauer M, Cote R, Duan L M, Jaksch D, Cirac J I, and Zoller P 2001 *Phys. Rev. Lett.* **87** 037901
[11] Gorshkov A V, Otterbach J, Fleischhauer M, Pohl T, and Lukin M D 2011 *Phys. Rev. Lett.* **107** 133602
[12] de Melo N R, Wade C G, Šibalić N, Kondo J M, Adams C S, and Weatherill K J 2016 *Phys. Rev. A* **93** 063863
[13] Fontaine Q, Bienaimé T, Pigeon S, Giacobino E, Bramati A, and Glorieux Q 2018 *Phys. Rev. Lett.* **121** 183604
[14] Zhang Z, Zhang Y, Sheng J, Yang L, Miri M A, Christodoulides D N, He B, Zhang Y, and Xiao M 2016 *Phys. Rev. Lett.* **117** 123601
[15] Liu B, Zhang L H, Ma Y, Wang Q F, Han T Y, Zhang J, Zhang Z Y, Shao S Y, Li Q, Chen H C, Guo G C, Ding D S, and Shi B S 2025 *Nat. Commun.* **16** 1419
[16] Chen C, Bornet G, Bintz M, Emperauger G, Leclerc L, Liu V S, Scholl P, Barredo D, Hauschild J, Chatterjee S, Schuler M, Läuchli A M, Zaletel M P, Lahaye T, Yao N Y, and Browaeys A 2023 *Nature* **616** 691

[17] Bernien H, Schwartz S, Keesling A, Levine H, Omran A, Pichler H, Choi S, Zibrov A S, Endres M, Greiner M, Vuletić V, and Lukin M D 2017 *Nature* **551** 579

[18] Ebadi S, Wang T T, Levine H, Keesling A, Semeghini G, Omran A, Bluvstein D, Samajdar R, Pichler H, Ho W W, Choi S, Sachdev S, Greiner M, Vuletić V, and Lukin M D 2021 *Nature* **595** 227

[19] Scholl P, Schuler M, Williams H J, Eberharter A A, Barredo D, Schymik K N, Lienhard V, Henry L P, Lang T C, Lahaye T, Läuchli A M, and Browaeys A 2021 *Nature* **595** 233

[20] Bloch I, Dalibard J, and Zwerger W 2008 *Rev. Mod. Phys.* **80** 885

[21] Zhang Z, Zhang Z, Han S, Zhang Y, Zhang G, Wu J, Sovkov V B, Liu W, Li Y, Zhang L, Xiao L, Jia S, Li W, and Ma J 2025 *npj Quantum Inf.* **11** 44

[22] Sedlacek J A, Schwettmann A, Kübler H, Löw R, Pfau T, and Shaffer J P 2012 *Nat. Phys.* **8** 819

[23] Wang Q, Liang Y, Wang Z, Guan S, Yang P, Zhang P, Li G, and Zhang T 2025 *Sci. China Phys. Mech. Astron.* **68** 264211

[24] An F A, Meier E J, and Gadway B 2017 *Sci. Adv.* **3** e1602685

[25] Chen T, Huang C, Velkovsky I, Hazzard K R A, Covey J P, and Gadway B 2024 *Nat. Commun.* **15** 2675

[26] Yu D, Song W, Wang L, Srikanth R, Sridhar S K, Chen T, Huang C, Li G, Qiao X, Wu X, Dong Z, He Y, Xiao M, Chen X, Dutt A, Gadway B, and Yuan L 2025 *Photonics Insights* **4** R06

[27] Huo M X, Nie W, Hutchinson D A W, and Kwek L C 2014 *Sci. Rep.* **4** 5992

[28] Chen T, Huang C, Velkovsky I, Ozawa T, Price H, Covey J P, and Gadway B 2025 *Nat. Phys.* **21** 221

[29] Gou W, Chen T, Xie D, Xiao T, Deng T S, Gadway B, Yi W, and Yan B 2020 *Phys. Rev. Lett.* **124** 070402

[30] Atala M, Aidelsburger M, Lohse M, Barreiro J T, Paredes B, and Bloch I 2014 *Nat. Phys.* **10** 588

[31] Mancini M, Pagano G, Cappellini G, Livi L, Rider M, Catani J, Sias C, Zoller P, Inguscio M, Dalmonte M, and Fallani L 2015 *Science* **349** 1510

[32] Stuhl B K, Lu H I, Aycock L M, Genkina D, and Spielman I B 2015 *Science* **349** 1514

[33] Livi L F, Cappellini G, Diem M, Franchi L, Clivati C, Frittelli M, Levi F, Calonico D, Catani J, Inguscio M, and Fallani L 2016 *Phys. Rev. Lett.* **117** 220401

[34] Cai H, Liu J, Wu J, He Y, Zhu S Y, Zhang J X, and Wang D W 2019 *Phys. Rev. Lett.* **122** 023601

[35] Gerbier F and Dalibard J 2010 *New J. Phys.* **12** 033007

[36] Wu X, Yang F, Yang S, Mølmer K, Pohl T, Tey M K, and You L 2022 *Phys. Rev. Res.* **4** L032046

[37] Cheng Y and Zhai H 2024 *Nat. Rev. Phys.* **6** 566

[38] Carr C, Ritter R, Wade C G, Adams C S, and Weatherill K J 2013 *Phys. Rev. Lett.* **111** 113901

[39] Scully M O and Zubairy M S 1997 *Quantum Optics* (Cambridge University Press)

[40] Steck D A "Rubidium 87 D Line Data" http://steck.us/alkalidata 2025 Revision 2.3.4, 8 August 2025

[41] Levine H J 2021 *Quantum Information Processing and Quantum Simulation with Programmable Rydberg Atom Arrays* Ph.D. thesis

[42] Preston D W 1996 *Am. J. Phys.* **64** 1432

[43] Scofield J H 1994 *Am. J. Phys.* **62** 129

[44] Goldman N, Budich J C, and Zoller P 2016 *Nat. Phys.* **12** 639